Frequency response of the superconducting gravimeter SG 056

Thomas Forbriger[1] and Alexandra Heck[2]

1   Geophysical Institute, Karlsruhe Institute of Technology, Black Forest Observatory (BFO), Germany
     E-Mail: Thomas.Forbriger@kit.edu
2   Geodetic Institute, Karlsruhe Institute of Technology, Germany
     E-Mail: Alexandra.Heck@kit.edu

Abstract

The two sensors of the SG 056 double-sphere superconducting gravimeter at BFO (Black Forest Observatory, Germany) show differences in their response to long-period seismic signals. Their frequency response deviates from the nominal GGP1-filter (8th-order Bessel low-pass). We experimentally derive parameterized models for the sensor's full frequency response by application of square-wave and down-sweep drive signals to the feedback circuit and subsequent inversion. The latter is carried out with the program `calex` in the time domain which iteratively minimizes the least-squares misfit between the output signal predicted with the filter model and the actual output of the sensor. We seek for values of eigenperiod and damping of the four 2nd-order subsystems of 8th-order low-pass filters. The resulting filters deviate considerably from the nominal response of the GGP1-filter also in that they are not Bessel filters. Remaining residuals indicate that the models are not able to capture the exact response. Nevertheless, they substantially reduce amplitudes of waveform-residuals in long-period earthquake recordings by a factor of four. The filter response curves approach their DC-limit (frequency $f = 0$ Hz) within the frequency band of the drive signals. Thus we estimate the asymptotic signal delay Δt_{DC} to be considered in tidal analysis to be $\Delta t_{\mathrm{DC}\,G1} = 10.44$ s for the lower sensor G1 (heavier sphere) and $\Delta t_{\mathrm{DC}\,G2} = 9.86$ s for the upper sensor G2 (standard sphere). The accuracy of these values appears to be not better than 0.07 s. For signals recorded with voltmeters on the UIPC data-acquisition and distributed through the IGETS data center (formerly GGP) $\Delta t_{\mathrm{DC}\,G1} = 9.84$ s and $\Delta t_{\mathrm{DC}\,G2} = 9.26$ s.

1   Introduction

Superconducting gravimeters (Prothero Jr. and Goodkind, 1968; Goodkind, 1999) are valuable for their exceptional stability and low drift (Crossley et al., 2013; Hinderer et al., 2007). They are the preferred instrument type for the observation of secular changes of gravity and tidal gravity signals. Widmer-Schnidrig (2003) demonstrated that they even outperform the most sensitive broad-band seismometers currently available at frequencies up to 1 mHz in the frequency-band of Earth's normal modes, if data are appropriately corrected for the effect of atmospheric masses (Zürn and Widmer, 1995). Rosat and Hinderer (2011) compared several superconducting gravimeters with respect to their noise-floor from the tidal frequency band to the frequencies of long period seismic signals. In the global comparison, the lower (heavier) sphere (sensor G1) of SG 056 at BFO provides the smallest background noise. Therefore it might not be surprising that Häfner and Widmer-Schnidrig (2013) were able to estimate the parameters of the free mode $_0S_2$ with unprecedented accuracy when using this instrument.

By design superconducting gravimeters provide an output voltage whose relation (amplitude and phase) to gravity is independent of frequency at large signal periods. The calibration factor for the amplitude (gain, sensitivity) commonly is obtained by comparison with readings of absolute gravity (Geib, 2010; Van Camp et al., 2016). The phase usually is expressed in terms of the asymptotic signal delay time for frequency $f = 0\,\mathrm{Hz}$ (DC), which is relevant for tidal analysis (Hinderer et al., 2007, sec. 3.04.2.4.4).

At smaller signal periods, in particular in the seismic frequency band, the roll-off of the instrument's frequency response becomes apparent. This becomes obvious in particular with instruments like SG 056 which contain two independent gravity sensors. The difference between both recorded gravity signals should vanish. While this is the case in the tidal frequency band, at smaller signal period, significant residuals remain for long-period seismic signals. The roll-off at higher frequency is expected to be primarily controlled by the low-pass filter in the output. Recent installations of superconducting gravimeters use an 8th-order Bessel low-pass, specified as GGP1-filter with a corner frequency of 61.5 mHz (Warburton, 1997).

The full frequency response is rarely determined for superconducting gravimeters in full detail. Van Camp et al. (2000) as well as Francis et al. (2011) analyze the step response and the phase shift of sinusoidal signals in the entire system after electromagnetic excitation. All instruments in their studies are equipped with a GGP1-filter. Van Camp et al. (2000) calibrated the SG-C021 at Membach (Belguim). They present diagrams for the frequency response in the period band from 3 s to 2000 s and extrapolate to DC where they specify $\Delta t_{DC} = (12.103 \pm 0.002)\,\mathrm{s}$ and $(12.101 \pm 0.003)\,\mathrm{s}$ as asymptotic delay time obtained with sine waves and step functions, respectively. Francis et al. (2011) investigated the response of OSG-CT40 (Walferdange, Luxembourg), SG-C021 (Membach, Belgium), and OSG-050 (Pecný, Czech Republic). They mistake the GGP1-filter for a Butterworth filter, but at the end even do not use a parametric model for an 8th-order low-pass. They use a transfer function with six poles and six zeroes to approximate the experimentally determined response and provide numerical values for the polynomial coefficients together with a graphical display of amplification and phase delay. Unfortunately

Δt_{DC} cannot easily be computed from the provided numbers. The presented frequency response, surprisingly, is non-monotonic with a maximum amplification and maximum phase delay near 10 mHz for all three instruments. For OSG-CT40 at a period of 2000 s they specify $\Delta t_{DC} = (8.281 \pm 0.020)\,\mathrm{s}$ and $(8.256 \pm 0.136)\,\mathrm{s}$ for sine waves and step functions, respectively. In the graphical display (Francis et al., 2011, Fig. 4b) the value for SG-C021 appears to be smaller than the value given by Van Camp et al. (2000) by more than 2.5 s, which might be due to a different data acquisition used in their setup.

The current contribution reports results of a detailed study of the frequency response for SG 056 (BFO, Germany) carried out by Heck (2014).

2   The instrument

The SG 056 is a dual-sphere instrument, where two sensors are confined in a single OSG-type dewar (Hinderer et al., 2007, Sec. 3.04.1.5.2). It was installed in September 2009 at the Black Forest Observatory (BFO) and is the first of its kind, where both sensors have a different probe mass. The heavier sphere (G1, lower sensor) has a mass of 17.7 g and the standard sphere (G2, upper sensor) has a mass of 4.34 g. Two different data acquisitions systems each record the signals of both sensors. Digital voltmeters (Agilent 34420A) take readings at a rate of one sample per second. These data are recorded by the so-called UIPC-system and are distributed through the IGETS data center (International Geodynamics and Earth Tide Service, 2017; Voigt et al., 2016). The secondary output of the sensors is connected to a Q330HR digitizer (Forbriger, 2011) which uses sigma-delta conversion and oversampling with a zero-phase FIR decimation filter. These data are distributed through the data management center of the Incorporated Research Institutions for Seismology (2017, network II, station BFO, channels BG1, BG2, LG1, and LG2).

The sensors in the superconducting gravimeter are operated in a force-balance feedback loop (Wielandt, 2012b) with an electromagnetic force transducer. This maintains the position of the probe mass with respect to the frame of the instrument by balancing forces acting on the probe mass. The output voltage of each sensor is directly proportional to the current in its feed-

Table 2.1: Characteristics of GGP1 filter intended for 1 Hz sampling rate as defined by GWR (literally copied from Warburton, 1997). The parameters of the GGP$_{\text{LP}}$-filter actually found in SG 056 (Tab. 5.1a) slightly differ from the nominal values.

– 8 pole Bessel filter
– Corner frequency at 61.5 mHz (16.3 sec period)
– Constant time delay of 8.2 seconds (Phase lag 0.034 deg/cpd)
– 100 dB attenuation at 0.5 Hz (f_{nyq} for 1 Hz sampling)
– Attenuation < 1% (-0.086 dB) below 0.01 Hz (100 sec period)
– Attenuation < 4% (-0.341 dB) below 0.02 Hz (50 sec period)

back coil and thus, at sufficiently large loop-gain, is a measure of external forces acting on the probe mass. The multi-slope integration analog-to-digital conversion of the digital voltmeters requires an appropriate analog anti-alias filter. This is provided by a low-pass filter with GGP1 characteristics (Tab. 2.1) in series to the sensor's output.

The nominal response function

$$
\begin{aligned}
T_{\text{nom}}(\omega) = \frac{\tilde{U}_{\text{r}}(\omega)}{\tilde{g}(\omega)} &= K\, T_{\text{GGP1}}(\omega) \\
&= \frac{K}{\displaystyle\prod_{k=1}^{4}\left(-\frac{T_{0,k}^2}{4\pi^2}\,\omega^2 + 2i\,h_k\,\frac{T_{0,k}}{2\pi}\,\omega + 1\right)}
\end{aligned}
\tag{2.1}
$$

of the instrument thus essentially is an eighth order low-pass Bessel filter. It relates the Fourier transform

$$
\tilde{g}(\omega) = \int\limits_{-\infty}^{+\infty} g(t)\, e^{-i\omega t}\, \mathrm{d}t
\tag{2.2}
$$

of the change in gravity $g(t)$ to the Fourier transform $\tilde{U}_{\text{r}}(\omega)$ of the recorded voltage by the response function $T_{\text{GGP1}}(\omega)$ of the GGP1 filter and the instrument's gain K. The eighth order Bessel filter can be factored into four 2nd-order systems. By analysis of the circuit diagram for the filters actually installed in SG 056, we obtain their nominal parameters for eigenperiod $T_{0,k}$ and damping h_k as a fraction of critical damping. They are closer to an eighth-order Bessel low-pass with $-3\,$dB corner frequency of 61.8 mHz than to the nominal GGP1-response. The parameters of this filter, which we call GGP$_{\text{LP}}$, are given in Tab. 5.1a. We assume their accuracy to be not better than 0.2 per cent. Of particular interest for tidal analysis is the asymptotic DC phase- and group-delay at frequency $f = 0\,$Hz which are both equal (Heck, 2014, sec. 6.2.2.3)

$$
\Delta t_{\text{DC}} = \sum_{k=1}^{4} \frac{h_k\, T_{0,k}}{\pi}.
\tag{2.3}
$$

3 Method of calibration

For the calibration of the frequency response we use the `calex`-procedure as described by Wielandt (2012b). The gravimeter in this case is excited electrically. In the case of the SG 056 we feed an electric current into the junction in front of the feedback driver. The current then is proportional to a force acting on the probe mass. Other than in broad-band seismometers, which provide a dedicated calibration coil, there not necessarily acts a force on the mechanical system. The feedback's controller can compensate the current equivalent to the force directly.

The significant benefit of exciting the instrument with an electric current is the possibility to record the very same current on the data acquisition system which is used to record the output of the instrument. Thus we know the excitation of the instrument very well (independent of the nature of the signal) and can compute the expected response in the output signal by digital signal processing based on a mathematical model for the instrument under investigation. The `calex`-procedure then minimizes the residual between the predicted output and the actually recorded response in a least-squares sense by iterative modification of the instrument's model parameters. Actually we solve an inverse problem. The remaining residual contains actual ground acceleration and gravity changes along with systematic remainders of the drive signal due to shortcomings of the mathematical model used to describe the sensor. We exemplify this approach in Fig. 3.1.

The program `calex`, which is available open source (Wielandt, 2012a; Wielandt and Forbriger, 2016), carries out the necessary computations. Wielandt (2012c) presents practical examples of its application. Starting at an initial model, `calex` does a local search in model space by application of a conjugate gradient algorithm. The user can control the condition number of the mis-

fit function by a kind of pre-conditioning (parameter 'unc', 'uncertainty', or 'search range' in the jargon of `calex`). This also affects the preferred down-hill direction.

Because SG 056 has two nearly identical sensors, we use the signal of sensor G1 to remove ground motion signals (at least partly) from the recording of sensor G2, before feeding the G2-signal to `calex`, and vice versa. This preprocessing is necessary because due to the instruments response the short-period background signals (marine microseisms) as well as the tidal signals occupy (by intention) a significant portion of the dynamic range. This is unfavorable for the calibration signal and causes a low signal-to-noise ratio if no correction would be applied.

4   Application to SG 056

We applied five test signals in total to the two sensors of SG 056 (Tab. 4.1). We alternatively use two different sources for the drive signal. The first source is offered by the controller of the SG 056 itself. It is a square wave signal of 20 minutes period (a fundamental signal frequency of 0.833 mHz, near the frequency of the fundamental radial free mode $_0S_0$) synchronized to recording time (a signal edge appears exactly at clock hour). We inject four cycles into the feedback loop for calibration of G1 and five for G2. The signal also is presented at an auxiliary output from where we record it on the seismological data acquisition system (Q330HR). The second source is an externally generated sine-wave down-sweep signal with a constant number of cycles per frequency decade (Wielandt, 1986) over about 3 decades. We inject the signal into the electronics of the SG 056 and record it on the seismological data acquisition (Q330HR) in parallel. All drive signals have a peak-to-peak amplitude of about 10 V. The differential buffer amplifier in front of the Q330HR doubles all voltages in the recordings. For the inversion we use data sampled synchronously from the gravity signal outputs G1 and G2 of SG 056 as well as the drive signal at a rate of 40 Hz by the Q330HR-digitizer. This keeps the Nyquist-frequency at a comfortable distance to the frequencies of interest at about 0.06 Hz, the -3 dB corner of the GGP$_{LP}$-filter.

The bandwidth of signals and simulation filters used for the inversion is limited by the anti-alias filter of `calex`, which we set to 2 Hz in the current case.

As initial model for the iterative inversion we use the nominal parameters for the GGP$_{LP}$-filter (Tab. 5.1a). All eight parameters of the 8th-order filter are used for optimization. Additionally we let `calex` adjust an amplitude factor and a small phase delay. The latter may account for a small delay produced by signal transducers or filters with corner-frequency outside the passband of the instrument and assumes only insignificant values of less than 1 ms in our case. The frequency response of the buffer amplifier in front of the Q330HR is ignored. Except for differential delay (Forbriger, 2011, about 0.14 ms due to component tolerance), which is too small to be significant here, the response of the buffer amplifier cancels in the `calex`-analysis, because it is similarly present in the recording of the drive signal as well as in the recorded output signal.

The ten degrees of freedom make the inverse problem inherently unstable and non-unique in the presence of noise in the signals. This goes along with trade-off between eigenperiod and damping of the four sub-systems. If not controlled by pre-conditioning, final models vary significantly and can contain unreasonable system parameters (poles on the imaginary ω-axis) without significant benefit for the residual rms (root-mean-square). After testing different adjustments (Heck, 2014, Abb. 5.6) we choose a configuration which favors a change in eigenperiod over a change in damping.

We obtain an improved set of filter parameters for each of the five test signals (Tab. 4.1) in the sense that the predicted output signal fits the recorded output signal with a significantly smaller rms residual. The rms-amplitude of the residual for signals predicted with the nominal GGP$_{LP}$ filter are about 5 per cent of the total signal for the square waves and 10 per cent to 24 per cent for the sweep signals. With the optimized filters the rms-amplitudes are less than 1 per cent in each of the cases and the variance always is reduced by more than 99 per cent.

To investigate the stability and significance of the obtained filter parameters, we compare the results for different drive signals at each sensor (Tab. 4.1). For dif-
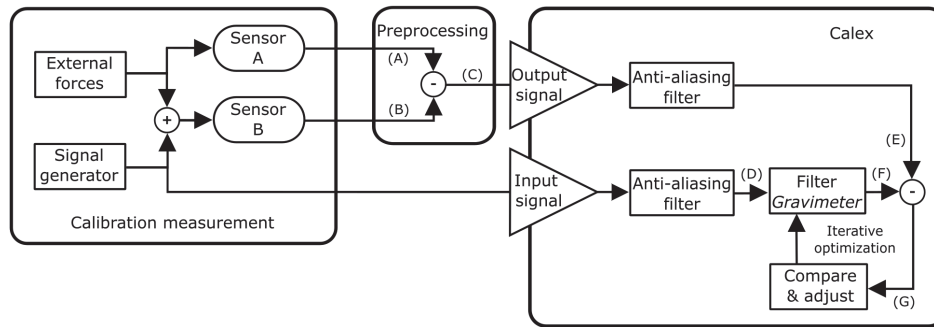
(a) Conceptual diagram of the calibration of instrument response with `calex` (Wielandt, 2012b). Examples of signals at labels (A to G) are displayed in diagram (b). Left box: The drive signal (*Signal generator*) is applied to *Sensor B* in this example and is recorded in parallel. Both sensors experience *External forces* (ground motion, gravity). Middle box: The recording of *Sensor A* (A), after appropriate scaling with the ratio of sensors gain values, is used to remove the external component at least partly from the output of the sensor under calibration (B). Their difference (C) primarily contains the response of *Sensor B* to the drive signal. Right box: `calex` simulates the sensor recording (*Output signal*) from the recording of the drive signal (*Input signal*). To both an identical *Anti-aliasing filter* is applied, which is necessary with the impulse-invariant recursive filters (Schüßler, 1981) used for system simulation. The output of the sensor is simulated from the drive signal (D) based on a model for the instrument's response (*Filter Gravimeter*). In the current study an eighth-order low-pass, an amplitude factor, and a signal delay are applied. Simulated output (F) and actual output (E) are compared and `calex` adjusts the filter parameters iteratively to minimize the residual (G) in a least-squares sense.
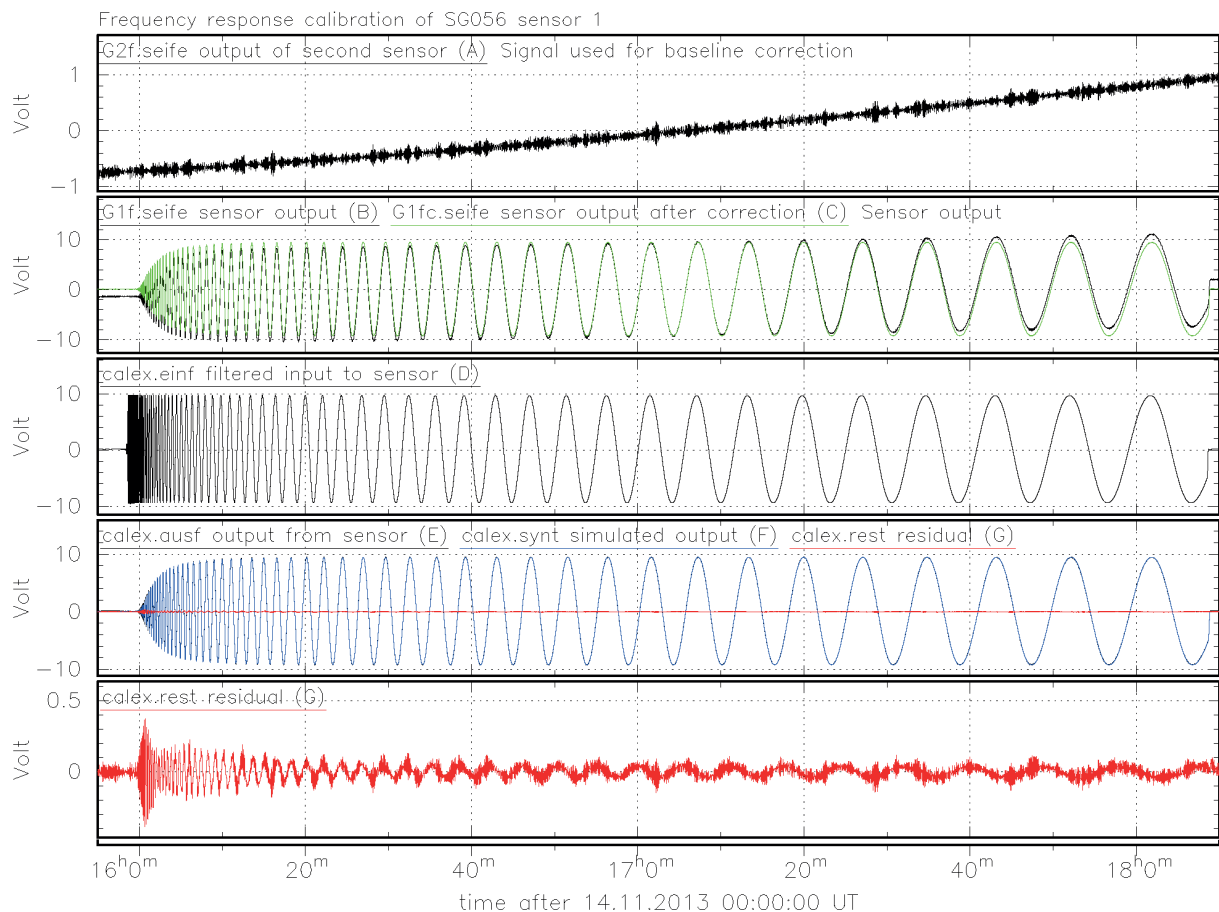
(b) Signals from the calibration of SG 056 sensor G1 with down-sweep 2 (Tab. 4.1). Labels (A to G) at the signals refer to the diagram (a). Panels from top to bottom: 1st panel: The recording of G2 (A) displays marine microseisms and tidal signals. 2nd panel: The signal of G2 is used to remove externally generated signals at least partly from the recording of G1 (B, black). The result (C, green) primarily shows the response of G1 to the drive signal. 3rd panel: Recording of the anti-alias filtered drive signal (D) which is understood as input to the sensor under calibration. 4th panel: The recorded output of G1 (E, black) is compared with the simulation (F, blue) and their residual (G, red). 5th panel: Display of the residual (G) at full scale.

Figure 3.1: Example of a complete `calex`-calibration analysis with a sweep-signal applied to sensor G1. (a) displays a conceptual diagram of the calibration recording with subsequent `calex`-inversion. Signals for the example are displayed in (b).

Table 4.1: Test signals used to drive the sensors of SG 056 in the calibration experiments.

sensor	signal	signal properties
G1	square-wave	20 minutes period; four cycles; duration 1 hour 20 minutes
G1	down-sweep 1	10 Hz to 10 mHz; duration about 1 hour; approximately 50 cycles per decade
G1	down-sweep 2	1 Hz to less than 2 mHz; duration about 2 hours; approximately 20 cycles per decade
G2	square-wave	20 minutes period; five cycles; duration 1 hour 40 minutes
G2	down-sweep	1 Hz to less than 2 mHz; duration about 2 hours; approximately 20 cycles per decade

ferent drive signals the filter parameters are reproduced within 1 per cent or less (Heck, 2014, Tab. 5.3). Compared to this, the variation of filter parameters due to different initial models is insignificant (Heck, 2014, Tab. 5.6). In the absence of a more elaborate measure, we take the variation between results for different drive signals as a lower limit for uncertainty.

Signal-residuals remain in particular at 10 s period in the band of marine microseisms (also with remainders of the drive signal) and for signal periods larger than 30 s. The minimum in the residual near 20 s might indicate that the chosen parameterization is not able to fit the actual response for smaller and larger periods simultaneously and that `calex` makes a compromise. An 8th-order low-pass filter apparently cannot exactly match the actual response. In addition to the `calex`-analysis we compute the frequency response function

$$T(\omega) = \frac{\tilde{U}_\mathrm{r}(\omega)\,\tilde{d}(\omega)^*}{\tilde{d}(\omega)\,\tilde{d}(\omega)^* + \varepsilon} \qquad (4.1)$$

from the Fourier transforms $\tilde{U}_\mathrm{r}(\omega)$ of the recorded output voltage and $\tilde{d}(\omega)$ of the drive signal, where $*$ means the complex conjugate and ε is a water-level for stabilization. It turns out that stabilization is not needed for the available signals. In contrast to the 8th-order filter, eq. (4.1) is not forced to a parameterized curvature. We obtain an independent value for each frequency ω.

5 Results

In Tabs. 5.1b and 5.1c we present the optimized parameters of the four 2nd-order subsystems for sensor G1 and G2, respectively. They are average values for the drive signals (Tab. 4.1) used with each sensor. Results

for different drive signals vary by 0.15 s for $T_{0,k}$ and by 0.0004 for h_k, at most, which gives a lower limit for uncertainty. The additional signal delay applied by `calex` is less than 1 ms in all cases (Heck, 2014, Tab. 8.1). We do not further discuss this delay because of its insignificance. All values for eigenperiod $T_{0,k}$ are significantly larger than those of the GGP$_\mathrm{LP}$-filter. Consequently the -3 dB corner frequencies of the optimized systems are smaller than those of the GGP$_\mathrm{LP}$-filter (Tab. 5.1). The filter parameters of G1 and G2 no longer represent Bessel-filters (Heck, 2014, Figs. 5.7 and 6.8). Also their asymptotic signal delay is larger than that of the GGP$_\mathrm{LP}$-filter in each case in Tab. 5.2.

In Fig. 5.1 we display the frequency response of the optimized models in comparison with the GGP$_\mathrm{LP}$-filter. While the phase delay and the group delay of the GGP$_\mathrm{LP}$-filter is constant at its asymptotic value for all frequencies smaller than the corner frequency f_c (a design-property of Bessel filters), this is not the case for the models found by calibration. The delay times are obviously frequency dependent at frequencies smaller than f_c. The sensors turn out to be dispersive in the seismic frequency band and consequently phase-delay (Tab. 5.2a) differs from group-delay (Tab. 5.2b) in this band. Although these effects are small, they definitely are a deviation from the response of a Bessel-filter.

Figs. 5.1a, 5.1b, and 5.1c give additional evidence that the 8th-order systems do not exactly match the actual response. The response obtained from Fourier transforms by eq. (4.1) is not precisely aligned with the curves for the parameterized models. The residual displayed in Fig. 3.1b gives a similar indication. However, deviation is small for both sensors when compared with the difference to the nominal GGP$_\mathrm{LP}$-filter.

(a) Frequency response for amplification.

(b) Frequency response for amplification.

(c) Frequency response for phase delay.

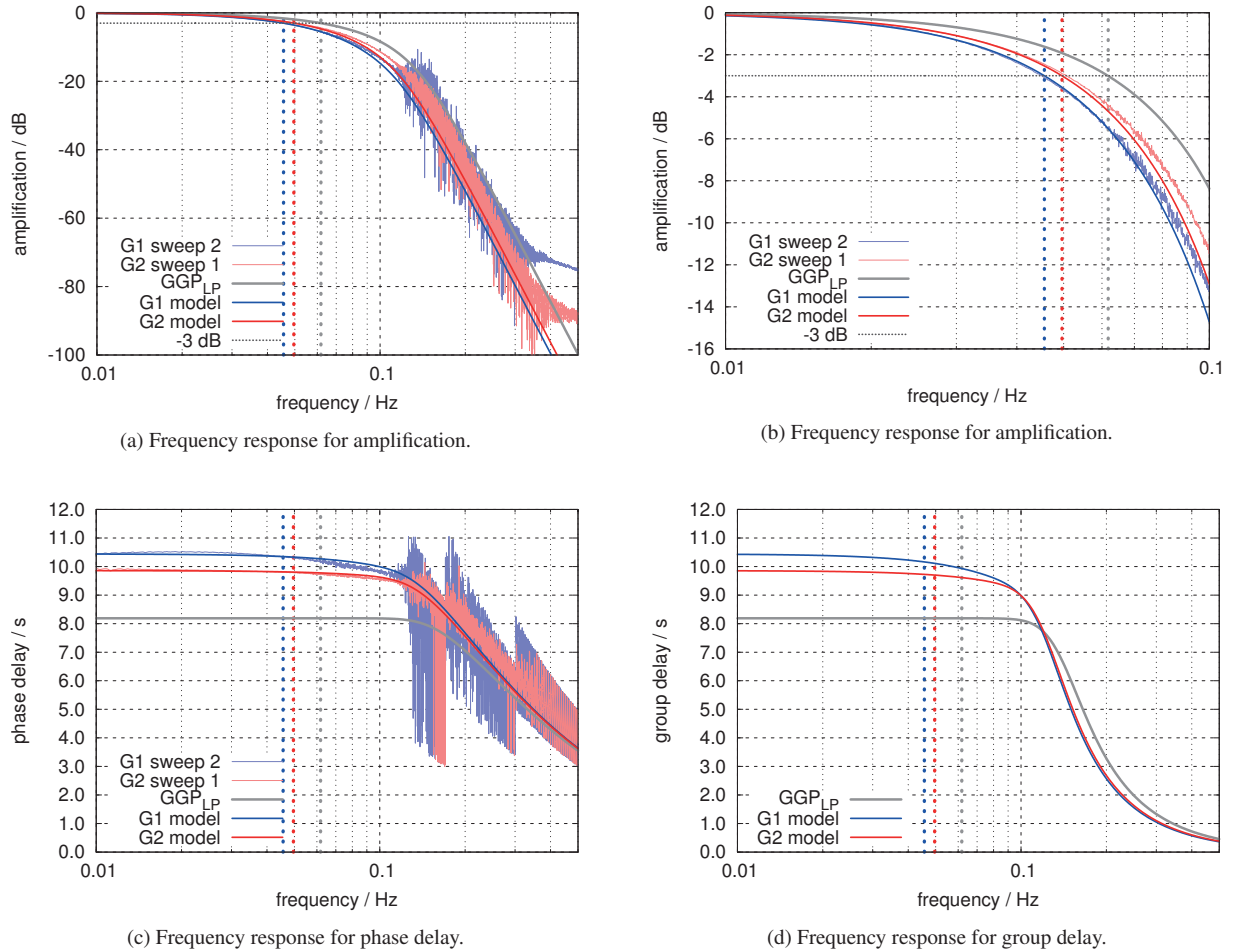(d) Frequency response for group delay.

Figure 5.1: Frequency response curves for the models presented in Tab. 5.1 (gray: GGP$_{LP}$ Tab. 5.1a, blue: G1 Tab. 5.1b, red: G2 Tab. 5.1c) and frequency response obtained from Fourier coefficients as defined in eq. (4.1) (light blue: G1 down-sweep 2 in Tab. 4.1, light red: G2 down-sweep) are shown additionally in the diagrams (a), (b), and (c). In (a) and (b) a horizontal, gray, dotted line indicates the level of -3 dB. Corner frequencies are read with respect to this level and are marked by vertical dashed lines in all diagrams.

At frequency larger than 0.11 Hz values from the ratio of Fourier coefficients suffer from the signal of microseisms present in the output of SG 056. As a consequence the signal-to-noise ratio for the calibration deteriorates. Values become unstable and in (c) partly suffer from phase-unwrapping artifacts.

Diagram (a) shows the stop-band properties for the GGP$_{LP}$-anti-alias-filter amplification dropping to -100 dB at Nyquist frequency. The response of the models found by calibration differs significantly from GGP$_{LP}$. At higher frequency they slightly underestimate signal amplitude (see also Fig. 5.2). The phase delay (c) and the group delay (d) differ from GGP$_{LP}$ in particular by about 2 s at the low-frequency limit. While both are flat to five digits for GGP$_{LP}$ for frequency smaller than corner frequency (Tab. 5.2), this property of the Bessel filter is missed by G1 and G2. At least the comparison with Fourier coefficients for G1 leaves some doubt, whether the curves approach the DC-limit for delay of the actual instrument.

Table 5.1: System parameters of 8th-order low-pass filters. The response is factorized into four 2nd-order subsystems. The properties of subsystem k are expressed in terms of eigenperiod $T_{0,k}$ and damping as a fraction h_k of critical, where angular eigenfrequency is $\omega_0 = 2\pi T_0^{-1}$. The poles of each factor of the respective subsystem in the response function (Fourier domain) as defined in eq. (2.1) are $\omega_{1,2} = 2\pi T_0^{-1}\left(ih \pm \sqrt{1-h^2}\right)$. The poles for the transfer function (Laplace domain) are $s_{1,2} = 2\pi T_0^{-1}\left(-h \pm i\sqrt{1-h^2}\right)$. We read the $-3\,\mathrm{dB}$ corner frequency f_c by eye from the amplitude response curve with an accuracy of 0.1 mHz. The asymptotic phase- and group-delay Δt_{DC} at DC (frequency $f = 0\,\mathrm{Hz}$) is defined by eq. (2.3). See Tab. 5.2 for phase- and group-delay of the filters at other values of frequency.

(a) defines the 8th-order Bessel low-pass derived from parameters of electronic components in the circuit diagram of the GGP$_\mathrm{LP}$-filters as implemented in SG 056. The parameters are expected to match the actual filters with an accuracy of at least 0.2 per cent.

(b) and (c) give the parameters for 8th-order low-pass (not Bessel) filters for the system response of sensor G1 and G2, respectively, of SG 056. The values are obtained by calibration and are optimal in the sense that they minimize the least-squares misfit to the calibration output signal. The values are averages for two (G2) or three (G1) different drive signals (Heck, 2014, Tab. 5.3). Results for different drive signals differ by 0.15 s for $T_{0,k}$, by 0.0004 for h_k, and by 0.07 s for Δt_{DC}, at most. If we disregard the results for down-sweep 1 on G1 (Tab. 4.1), the variation of Δt_{DC} reduces to $\pm 0.007\,\mathrm{s}$. When using Δt_{DC} with data recorded by the UIPC system, values must by reduced by 600 ms in both cases because the voltmeters apparently advance signals (see Section 6).

(a) GGP$_\mathrm{LP}$-filter as implemented in the electronics of SG 056.

k	$T_{0,k}$ / s	h_k
1	9.09897	0.98806
2	8.83175	0.89355
3	8.28409	0.70338
4	7.39218	0.40802

$$f_c = 0.0618\,\mathrm{Hz}$$
$$\Delta t_{\mathrm{DC}} = 8.1885\,\mathrm{s}$$

(b) Model for the response function of sensor G1 as estimated with `calex`.

k	$T_{0,k}$ / s	h_k
1	11.850	0.99070
2	11.415	0.89625
3	10.394	0.70609
4	8.506	0.41040

$$f_c = 0.0456\,\mathrm{Hz}$$
$$\Delta t_{\mathrm{DC}} = 10.4407\,\mathrm{s}\,(-0.6\,\mathrm{s})$$

(c) Model for the response function of sensor G2 as estimated with `calex`.

k	$T_{0,k}$ / s	h_k
1	11.077	0.98980
2	10.701	0.89530
3	9.884	0.70514
4	8.432	0.40970

$$f_c = 0.0496\,\mathrm{Hz}$$
$$\Delta t_{\mathrm{DC}} = 9.8577\,\mathrm{s}\,(-0.6\,\mathrm{s})$$

Table 5.2: Values of delay time as computed for system parameters listed in Tab. 5.1. For a Bessel-filter like GGP$_\mathrm{LP}$ the delay is practically independent of frequency for values smaller than the $-3\,\mathrm{dB}$ corner frequency f_c. The system response derived by calibration for sensor G1 and G2 significantly differs from a Bessel low-pass in this respect. Delay times with filter parameters optimized for different drive signals differ by 0.07 s at most.

(a) Phase delay in seconds.

	frequency f			
	$\to 0\,\mathrm{Hz}$	$0.001\,\mathrm{Hz}$	$0.01\,\mathrm{Hz}$	f_c
GGP$_\mathrm{LP}$	8.1885	8.1885	8.1885	8.1885
G1	10.4407	10.4407	10.4362	10.3476
G2	9.8577	9.8577	9.8555	9.8054

(b) Group delay in seconds.

	frequency f			
	$\to 0\,\mathrm{Hz}$	$0.001\,\mathrm{Hz}$	$0.01\,\mathrm{Hz}$	f_c
GGP$_\mathrm{LP}$	8.1885	8.1885	8.1885	8.1882
G1	10.4407	10.4406	10.4272	10.1622
G2	9.8577	9.8576	9.8513	9.7009

6 Intricacies of the UIPC-digitizer

Data recorded with the UIPC-digitizer present gravity with a delay reduced by 600 ms. This system makes use of two high-precision digital voltmeters to convert voltage to a digital representation of the value. They are multi-slope integration analog-to-digital converters. To come as close as possible to DC accuracy, the voltmeters take a reference reading (auto zero) prior to each data sample. The voltmeters take 400 ms for the zero reading and 400 ms for the data conversion. In consequence the centroid of the time window when the actual data sample is taken is delayed by 600 ms with respect to the wall clock second and thus also to time indicated in the data file for the respective sample

(GWR Instruments, 2011). This value was confirmed by the phase shift between signals recorded with the UIPC-system on the one hand and the Q330HR-system on the other hand. Thus all signal delay is effectively reduced by 0.6 s in data presented by the UIPC-system.

7 Discussion and Conclusions

The filter parameters we found by calibration of sensor G1 (Tab. 5.1b) and G2 (Tab. 5.1c) differ from parameters of the electronic low-pass GGP$_\mathrm{LP}$-filter (Tab. 5.1a) by up to 30 per cent. In return they capture the response of SG 056 significantly better than the nominal values. This is true even though remaining residuals indicate, that the actual response of the sensors is not exactly

captured by the eight poles. In the calibration procedure signal variance was reduced by more than 99 per cent.

The remaining residual as well as the deviation of the parameterized models from values obtained by Fourier transformation in Fig. 5.1 might indicate that the models in Tab. 5.1 are primarily optimal for the drive signals we chose. In Fig. 5.2 we demonstrate an application of the calibration result to recorded ground motion of earthquake body-waves, although we do not intend to use SG 056 for observation of that type of signal. With the system parameters as given in Tab. 5.1 we reduce the waveform-residuals to the reference signal (recorded with a broad-band seismometer) as well as the waveform-residual between sensor G1 and G2 by about a factor of four.

We do not expect the actual implementation of the GGP_{LP}-filter to be the cause of the deviation from the nominal response. While some of the sensor parameters deviate up to 30 per cent from GGP_{LP}, electronic circuitry can be constructed with an accuracy at the level of 0.1 per cent and the GGP_{LP} Bessel filter specified in Tab. 5.1a matches the values obtained from circuit analysis by 0.2 per cent or better. Further, we repeated the calibration with a set of replacement boards for the gravity cards in the GEP (gravimeter electronics package). This confirmed the results presented here, such that the deviation must be due to a different cause and not to component tolerance. In our opinion, the deviation is caused by the loop-gain of the feedback system becoming finite and rather small near the corner frequency of the GGP_{LP}-filter. This hypothesis is supported by a rather large amplitude of the error signal in the feedback control at frequencies of a few 100 mHz. With small loop-gain the effective response of the mechanical system (superconducting probe mass levitated in magnetic field) gains influence in the overall system response. This cause still has to be confirmed by additional experiments with the open loop system and a computation of the overall theoretical feedback response.

The studies by Van Camp et al. (2000) and Francis et al. (2011) as well show significant deviations from the nominal response of a GGP1-filter. However, the frequency response curves presented by Francis et al. (2011) are arguable in that they result from a parameterization with six poles and six zeroes, which apparently produces a non-monotonic response with a maximum amplification and maximum phase delay near 10 mHz for all three instruments under investigation. The value of $\Delta t_{DC} = 12.1$ s presented by Van Camp et al. (2000) for SG-C021 is larger than the value we obtain for SG 056. However, according to the authors, a delay of 2.635 s in the data acquisition contributes to this. This appears in agreement with curves showing a smaller delay than presented by Francis et al. (2011, Fig. 4b) for the same instrument recorded on a Quanterra 330 data logger. The accuracy of ± 0.003 s claimed by Van Camp et al. (2000) for the delay determined for the GGP1-output with a less then 3 minutes long step signal may appear surprisingly small when compared with results for other instrument outputs in the same study.

The parameterized filters which we obtain for the two sensors of SG 056 approach their asymptotic signal delay Δt_{DC} within the bandwidth of the drive signals of calibration in the accuracy-margin of 0.07 s (Tab. 5.2). However, in particular for G1 we observe a deviation for signal delay computed from Fourier transforms (Fig. 5.1c). This may challenge the applicability of Δt_{DC} given in Tab. 5.1 for the delay tidal signals experience in the actual systems. We therefore test, whether we can recover the differential delay of 0.58 s for which signals of G1 appear later than signals recorded with G2 using a tidal analysis with Eterna 3.40 (Wenzel, 1996). Eva Schroth carried out the analysis of high-pass filtered data and provides us with tidal parameters for the diurnal and semi-diurnal wave-groups. She used recordings from January 1, 2010 to March 30, 2016 which were not corrected with respect to nominal delay. The phase residuals between sensors G1 and G2 for the major tidal wave groups (O1, P1, K1, and M2) are about 0.21 s to 0.32 s and of the expected sign. Standard deviation as computed by Eterna for a band-limited noise model are larger than 0.42 s in all cases. The differences between models for G1 and G2 as given in Tab. 5.1 may therefore be insignificant to tidal analysis. The deviation from the nominal delay of 8.2 s, however, is significant. Riccardi et al. (2012, Tab. 2) present a similar analysis with slightly more than four months of data, only. Consequently their values of standard deviation are considerably larger.
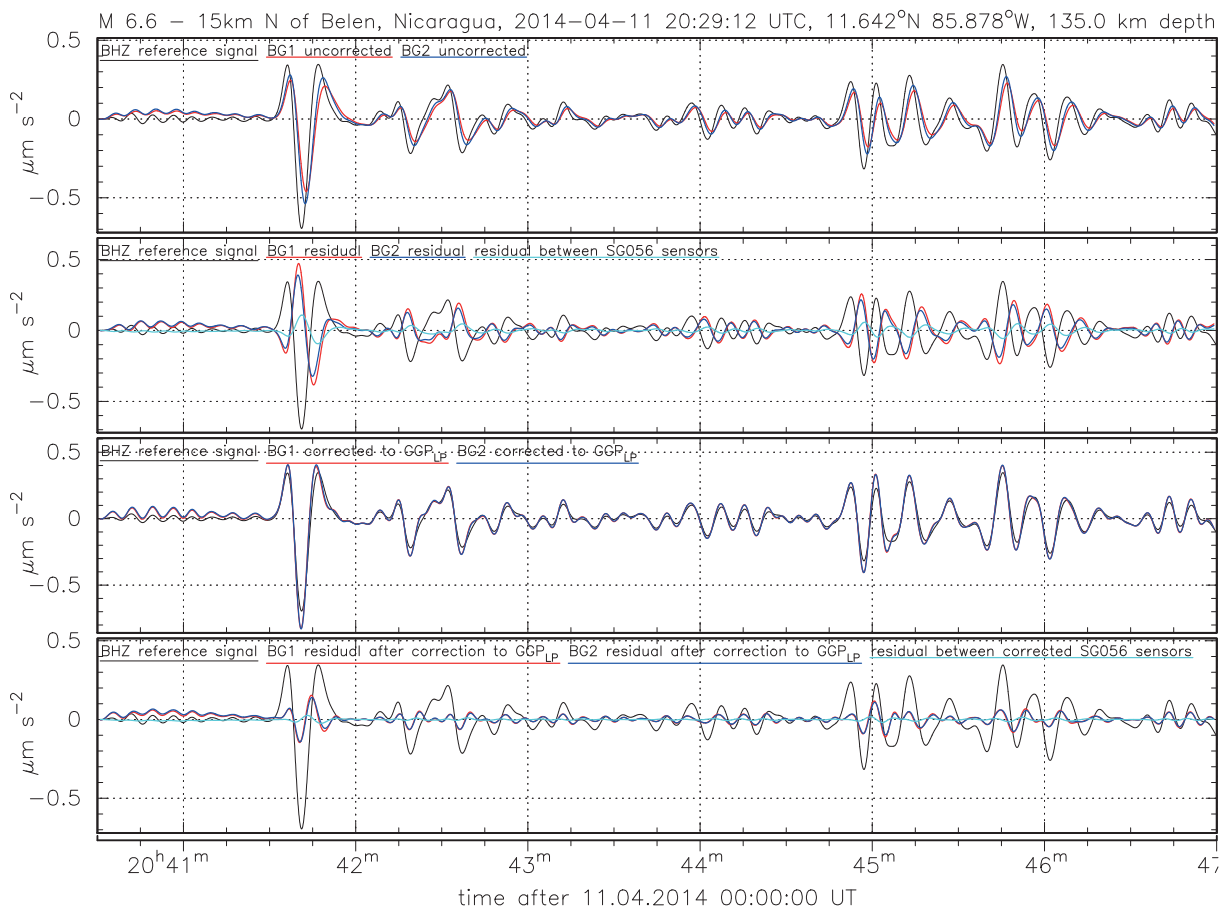
Figure 5.2: Recordings of long-period body-wave signals (P 20:41:30, PP 20:44:45) of a magnitude 6.6 earthquake in Nicaragua. We use this recording to test the usefulness of the response models (Tab. 5.1) in application to ground motion data.

BHZ (black): recording of the STS-2 seismometer's vertical component at BFO. BG1 (red) and BG2 (blue): recordings of SG 056 sensors G1 and G2, respectively. cyan: difference between SG 056-sensors (G1-G2).

The BHZ-signal is converted to acceleration and the GGP$_{LP}$-filter is applied to the recording. Similarly the STS-2-response (2nd-order high-pass with eigenperiod $T_0 = 120\,$s and $h = 0.719$ of critical damping) is applied to the signals of G1 and G2 such that all three represent ground acceleration in the frequency band from about $8.3\,$mHz to about $62\,$mHz.

Top two panels: Only the STS-2-high-pass is applied to G1 and G2, but no further correction. Bottom two panels: The response of G1 and G2 additionally is corrected by an equalizer from the parameters given in Tab. 5.1b and 5.1c, respectively, to GGP$_{LP}$ (Tab. 5.1a). The first and third panel (from the top) display the actual recording of ground motion. The second and fourth panel display the reference signal (LHZ, black) together with the residuals with respect to the reference (red, blue) and the difference between the two sensors of SG 056 (G1-G2, cyan).

Without correction G1 and G2 show shortcomings not only in amplitude, but in signal phase in particular. The correction to the GGP$_{LP}$-response fixes the phase and slightly overestimates amplitude. The remaining residuals are of higher frequency. When expressing the peak-to-peak amplitude of the P-wave waveform residual with respect to the reference signal, the correction reduces the residual from almost 90 per cent to 30 per cent. The difference G1-G2 is reduced from 20 per cent to less than 5 per cent.

Acknowledgments

References

Crossley, D., Hinderer, J., and Riccardi, U. (2013): The measurement of surface gravity. *Reports on Progress in Physics* 76(4):046101. DOI: 10.1088/0034-4885/76/4/046101.

Forbriger, T. (2011): Buffer amplifier for SG-056 signals to Q330HR. Technical report. unpublished. Black Forest Observatory (BFO). URL: http://nbn-resolving.org/urn:nbn:de:swb:90-741065 (visited on 11/28/2017).

Francis, O., Lampitelli, C., Klein, G., Van Camp, M., and Pálinkáš, V. (2011): Comparison between the Transfer Functions of three Superconducting Gravimeters. *Bull. Inf. Marées Terrestres.* 147:11857–11868. URL: http://www.bim-icet.org/ (visited on 09/18/2017).

Geib, T. (2010): Genauigkeit der in-situ Kalibrierung des supraleitenden Gravimeters SG-056 am BFO. German. Accuracy of the in-situ calibration of the superconducting gravimeter SG-056 at BFO. Diploma thesis. Karlsruhe Institute of Technology (KIT), Geophysical Institute, Germany. URL: http://nbn-resolving.org/urn:nbn:de:swb:90-466628.

Goodkind, J. M. (1999): The superconducting gravimeter. *Review of Scientific Instruments* 70(11):4131–4151. DOI: 10.1063/1.1150092.

GWR Instruments (2011): DAC-3: Data Acquisition Controller Description and Installation Procedures. unpublished system documentation, 2011-08-03.

Häfner, R. and Widmer-Schnidrig, R. (2013): Signature of 3-D density structure in spectra of the spheroidal free oscillation $_0S_2$. *Geophysical Journal International* 192(1):285–294. DOI: 10.1093/gji/ggs013.

Heck, A. (2014): Bestimmung des Frequenzgangs des supraleitenden Gravimeters SG056. German. Frequency response calibration of the superconducting gravimeter SG056. Bachelor thesis. Karlsruhe Institute of Technology (KIT). URL: http://nbn-resolving.org/urn:nbn:de:swb:90-466570.

Hinderer, J., Crossley, D., and Warburton, R. J. (2007): Gravimetric Methods - Superconducting Gravity Meters. In: *Geodesy*. Ed. by G. Schubert. Vol. 3. Treatise on Geophysics. Elsevier B.V. Chap. 3.04, pp. 65–120. DOI: 10.1016/B978-044452748-6.00172-3.

Incorporated Research Institutions for Seismology (2017): IRIS DMC MetaData Aggregator for Station II/BFO. data centre. URL: http://ds.iris.edu/mda/II/BFO (visited on 09/19/2017).

International Geodynamics and Earth Tide Service (2017): The IGETS data base at GFZ Potsdam. data centre. URL: http://isdc.gfz-potsdam.de/igets-data-base/ (visited on 10/19/2017).

Prothero Jr., W. A. and Goodkind, J. M. (1968): A Superconducting Gravimeter. *Review of Scientific Instruments* 39(9):1257–1262. DOI: 10.1063/1.1683645.

Riccardi, U., Rosat, S., and Hinderer, J. (2012): On the Accuracy of the Calibration of Superconducting Gravimeters Using Absolute and Spring Sensors: a Critical Comparison. *Pure and Applied Geophysics* 169:1343–1356. DOI: 10.1007/s00024-011-0398-8.

Rosat, S. and Hinderer, J. (2011): Noise Levels of Superconducting Gravimeters: Updated Comparison and Time Stability. *Bull. Seism. Soc. Am.* 101(3):1233–1241. DOI: 10.1785/0120100217.

Schüßler, H.-W. (1981): A Signalprocessing Approach to Simulation. *Frequenz* 35(7):174–184. DOI: 10.1515/FREQ.1981.35.7.174.

Van Camp, M., Meurers, B., de Viron, O., and Forbriger, T. (2016): Optimized strategy for the calibration of superconducting gravimeters at the one per mille level. *Journal of Geodesy* 90(1):91–99. ISSN: 0949-7714. DOI: 10.1007/s00190-015-0856-7. URL: http://dx.doi.org/10.1007/s00190-015-0856-7.

Van Camp, M., Wenzel, H.-G., Schott, P., Vauterin, P., and Francis, O. (2000): Accurate transfer function determination for superconducting gravimeters. *Geophysical Research Letters* 27(1):37–40. DOI: 10.1029/1999GL010495.

Voigt, C., Förste, C., Wziontek, H., Crossley, D., Meurers, B., Pálinkáš, V., Hinderer, J., Boy, J.-P., Barriot, J.-P., and Sun, H. (2016): Report on the Data Base of the International Geodynamics and Earth Tide Service (IGETS). Tech. rep. Scientific Technical Report STR - Data; 16/08. Potsdam, Germany: GFZ German Research Centre for Geosciences, p. 24. DOI: 10.2312/GFZ.b103-16087.

Warburton, R. (1997): Optimizing the Performance of the SG during the GGP. Presentation at First GGP Workshop. URL: http://www.eas.slu.edu/GGP/gwrwrk1.html (visited on 09/21/2017).

Wenzel, H. G. (1996): The nanogal software: Earth tide data processing package ETERNA 3.30. *Bulletin d'Information des Marées Terrestres* 124:9425–9439. URL: http://www.bim-icet.org/ (visited on 12/07/2017).

Widmer-Schnidrig, R. (2003): What can superconducting gravimeters contribute to normal-mode seismology? *Bull. Seism. Soc. Am.* 93(3):1370–1380. DOI: 10.1785/0120020149.

Wielandt, E. (1986): Circuit diagram for a down-sweeper with constant number of cycles per decade. URL: http://www.software-for-seismometry.de/lectures/calib-c/figures/Sweeper-Circuit-c.jpg (visited on 10/20/2017).

Wielandt, E. (2012a): Program CALEX. open source software. URL: http://www.software-for-seismometry.de/software/calex/ (visited on 09/18/2017).

Wielandt, E. (2012b): Seismic Sensors and their Calibration. In: *New Manual of Seismological Observatory Practice 2 (NMSOP-2)*. Ed. by P. Bormann. Technical Report. Potsdam, Germany: GeoForschungsZentrum GFZ, pp. 1–51. DOI: 10.2312/GFZ.NMSOP-2_ch5.

Wielandt, E. (2012c): Seismometer calibration with program CALEX. In: *New Manual of Seismological Observatory Practice 2 (NMSOP-2)*. Ed. by P. Bormann. Exercise 5.4. Potsdam, Germany: GeoForschungsZentrum GFZ, pp. 1–3. DOI: 10.2312/GFZ.NMSOP-2_EX_5.4.

Wielandt, E. and Forbriger, T. (2016): Linux version of program CALEX. open source software. URL: https://git.scc.kit.edu/Seitosh/software-for-seismometry-linux/tree/master/software/calex (visited on 09/18/2017).

Zürn, W. and Widmer, R. (1995): On noise reduction in vertical seismic records below 2 mHz using local barometric pressure. *Geophysical Research Letters* 22(24):3537–3540. DOI: 10.1029/95GL03369.